LETTER Communicated by Andrey Shilnikov

Predicting the Existence and Stability of Phase-Locked Mode in Neural Networks Using Generalized Phase-Resetting Curve

Sorinel A. Oprisan
oprisans@cofc.edu
College of Charleston, Department of Physics and Astronomy, Charleston, SC 29424, U.S.A.

We used the phase-resetting method to study a biologically relevant three-neuron network in which one neuron receives multiple inputs per cycle. For this purpose, we first generalized the concept of phase resetting to accommodate multiple inputs per cycle. We explicitly showed how analytical conditions for the existence and the stability of phase-locked modes are derived. In particular, we solved newly derived recursive maps using as an example a biologically relevant driving-driven neural network with a dynamic feedback loop. We applied the generalized phase-resetting definition to predict the relative-phase and the stability of a phase-locked mode in open loop setup. We also compared the predicted phase-locked mode against numerical simulations of the fully connected network.

1 Introduction

All organisms have developed adaptation mechanisms in order to survive. Environmental stimuli such as light constantly reset the endogenous rhythms of organisms, such as those generated by the circadian clock (Winfree, 2001; Refinetti, 2005). Stimuli-induced resetting in neuronal oscillators has important biological functions in visual perception (Vetter, Haynes, & Pfaff, 2000; Romei, Gross, & Thut, 2012), memory (Barnes, Suster, Shen, & McNaughton, 1997; Kirillov, Myre, & Woodward, 1993), representation of temporal durations (Okamoto & Fukai, 2000; Oprisan & Buhusi, 2011, 2013a, 2013b, 2014; Buhusi & Oprisan, 2013; Oprisan, Dix, & Buhusi, 2014), sleep and arousal (McCormick & Bal, 1997), and learning (Lisman, 1997; Oprisan, Lynn, Tompa, & Lavin, 2015).

An important class of biologically relevant applications of phase resetting in neural oscillators is the prediction of phase-locked modes in central pattern generators (CPGs), which are autonomous neural networks capable of producing multiphase rhythms underlying motor behaviors, such as those responsible for heartbeat, respiratory functions and locomotion

Neural Computation **29, 2030–2054** (2017)
doi:10.1162/NECO_a_00983

(Selverston, 1987; Marder & Calabrese, 1996; Eken, Hultborn, & Kiehn, 1989), and sensory processing (Gray, 1995; Laurent, 1996).

Motivated by experimental studies of swim CPGs of the sea slugs *Melibe leonina* and *Dendronotus iris* (Sakurai, Gunaratne, & Katz, 2014), extensive numerical studies using three-neuron motifs were developed for the purpose of modeling different rhythmic patterns (Shilnikov, Gordon, & Belykh 2008; Alacam and Shilnikov, 2015). Through direct numerical integration of model equations based on the realistic Plant model of the R15 neuron in *Aplysia Californica* (Plant & Kim, 1976), numerical simulations of fully coupled networks led to multistable patters similar to experimental data (Alacam & Shilnikov, 2015).

Another extensively studied three-neuron motif contained generic and identical FitzHugh-Nagumo relaxation oscillators (FitzHugh, 1955; Nagumo, Arimoto, & Yoshizawa, 1962) with all-to-all coupling (Schwabedal, Knapper, & Shilnikov, 2016). By phase reduction, bifurcation and perturbation analysis, and stochastic dynamics, they mapped a wide range of parameter space and identified relevant network multistable phase-locked modes (Schwabedal et al., 2016).

Conceptually, unidirectional coupling between neural oscillators (i.e., a driving-driven system) is the simplest possible synchronization mechanism that uses phase resetting to drive a neural population to a desired phase-locked firing pattern. Phase-resetting methodology has been successfully used for predicting one-to-one entrainment in networks where the receiving population always follows the driving population (Oprisan & Canavier, 2002a, 2002b; Oprisan, Thirumalai, & Canavier, 2003; Oprisan, Prinz, & Canavier, 2004). Unidirectional coupling also allows for "anticipated synchronization" (Voss, 2000) in which the receiving population anticipates the states of the driving population (Calvo, Chialvo, Eguiluz, Mirasso, & Toral, 2004). It has been analytically proven and numerically verified that time-delayed feedback can produce multistable phase-locked modes (Oprisan & Canavier, 2003) or force-coupled dynamical systems onto a synchronization manifold that involves the future state of the drive system, that is, anticipating synchronization (Voss, 2000). Such anticipating synchronization is counterintuitive since the future evolution of the drive system is anticipated by the response system despite the unidirectional coupling. It has been suggested that delayed coupling in dynamical systems separated by some distance can still promote synchronization despite the slow signal transmission and the unidirectional coupling. The first anticipating synchronization study of excitable systems was done by (Ciszak, Calvo, Masoller, Mirasso, & Toral, 2003), followed by more recent behavioral-related investigations (Stepp & Turvey, 2010; Stephan, Zilles, & Kotter, 2000). Furthermore, synaptic delay and synaptic plasticity were recently extensively investigated as potential control parameters that can lead to tunable delayed and anticipating synchronization in neural networks

(Sausedo-Solorio & Pisarchik, 2014; Simonov, Gordleeva, Pisarchik, & Kazantsev, 2014; Matias, Carelli, Mirasso, & Copelli, 2015).

We investigated analytically and numerically a three-neuron driving-driven system with a dynamic inhibitory loop that was shown to exhibit anticipating synchronization (Matias, Carelli, Mirasso, & Copelli, 2011; Matias, 2014; Matias et al., 2014). The three-neuron network investigated here was shown to produce both delayed synchronization, in which presynaptic neuron fires a spike before postsynaptic neuron, and anticipating synchronization. It was argued that the delayed synchronization under spike-timing-dependent plasticity rules facilitates long-term potentiation (Matias et al., 2015), whereas anticipating synchronization could contribute to long-term depression of synaptic couplings (Matias, 2014; Matias et al., 2011, 2014, 2015).

This study focuses on deriving analytic criteria for the existence and the stability of phase-locked modes in this three-neuron network (see Matias et al., 2011, 2014). For this purpose, we used the method of phase resetting, or response, curve (PRC) (Oprisan et al., 2004; Oprisan & Canavier, 2005; Oprisan & Boutan, 2008; Oprisan, 2009, 2010, 2012a, 2012b, 2013, 2014a). The novelties of this study are (1) the generalization of phase resetting to multiple inputs per cycle and (2) the prediction of phase-locked modes in a neural network that is no longer limited to one-to-one firing patterns. Throughout the letter, the neurons are labeled as 1 for the driving neuron, 2 for the driven neuron, and 3 for the neuron of the feedback loop. The driven neuron 2 receives two inputs during the same cycle: one excitatory input from the driving neuron 1 and one inhibitory input from the feedback loop represented by neuron 3. The synaptic couplings are labeled with two indices, the first representing the pre- and the second the postsynaptic neuron. For example, g_{12} stands for the strength of the synaptic coupling from neuron 1 to neuron 2.

2 Phase-Resetting Curve Method

The PRC method has been extensively used for predicting phase-locked modes in neural networks (Mirollo & Strogatz, 1990; Perkel, Schulman, Bullock, Moore, & Segundo, 1964; Winfree, 1989, 2001). It assumes that the only effect of a presynaptic stimulus is to reset the phase of the ongoing oscillation of a neuron. Traditionally, the PRC tabulates the transient change in the firing frequency of a neural oscillator in response to one external stimulus per cycle of oscillation (see Figure 1a). Recently we suggested a generalization of the PRC to account for the overall resetting when two or more inputs are delivered during the same cycle (see Figure 1c; Vollmer, Vanderweyen, Tuck, & Oprison, 2015), which was further developed in this study. As a result, we expanded the range of applications of the PRC theory from the prediction of the traditional one-to-one phase-locked modes to arbitrary phase-locked firing patterns. Here we present a quantitative

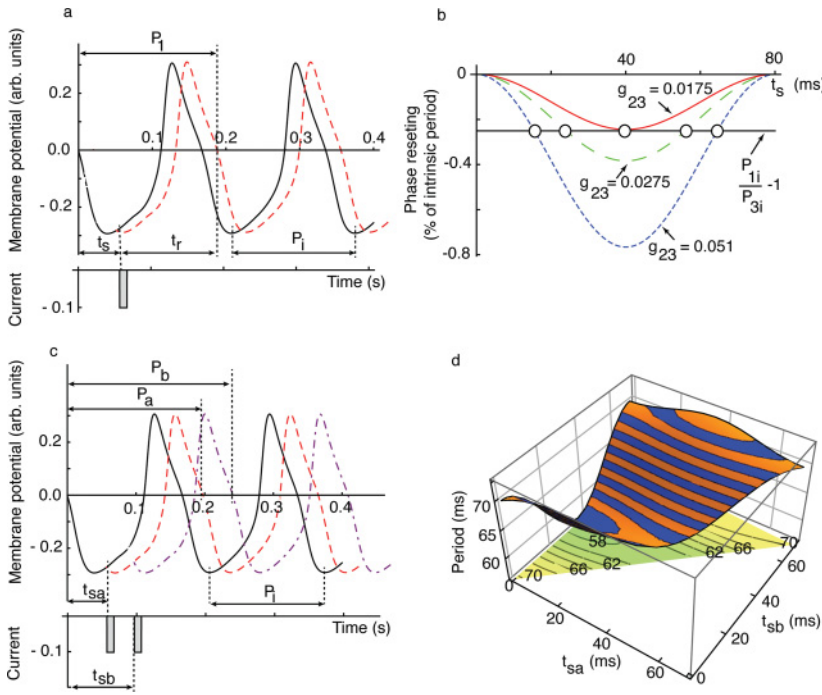

Figure 1: Single- and multiple-stimuli PRCs. (a) A free-running neural oscillator (continuous line) with an intrinsic period P_i is perturbed at stimulus time t_s by a brief current pulse (see the shaded rectangle). As a result, the perturbed oscillation (dashed line) has a transiently modified period P_1, which induces a phase shift of all subsequent spikes. (b) The amount of phase resetting depends on its timing (phase) and the pre- to postsynaptic coupling strength g. A coupling weaker than $g_{23} = 0.0175$ (arb. units) cannot bring neuron 3 from its intrinsic firing period P_{3i} to the common firing period P_{1i} of the driving neuron. (c) Two brief stimuli delivered at stimulus times t_{sa} and, respectively, t_{sb} produced cumulative effects. The first stimulus transiently modified the intrinsic firing period P_i to a new value P_a, and the second stimulus further resets the firing period to P_b. (d) A typical two-stimuli phase response surface for a class I excitable cell. Since the PRC in response to two stimuli depends on both t_{sa} and t_{sb}, the phase resetting becomes a three-dimensional surface.

analysis of phase-locked modes prediction based on the newly introduced generalized PRC.

We measured all durations from an arbitrary phase reference $\varphi = 0$, which was the zero crossing of the membrane potential with a positive slope. The time between the most recent crossing of the phase reference and the moment of stimulus activation is called stimulus time t_s. The duration

between a stimulus and the next crosses of the phase reference is called recovery time t_r. In the case of a single stimulus, the PRC measures the percentage change of the firing period from its free running value P_i to a transiently modified value P_1 (see Figure 1a):

$$F^{(1)}(\varphi) = P_1/P_i - 1, \tag{2.1}$$

where the superscript $^{(1)}$ emphasizes that the phase resetting is due to a single input per cycle, which has been the classic definition of PRC. The stimulus phase is defined as $\varphi = t_s/P_i$. To simplify the notation, throughout the rest of the letter, we drop the superscript $^{(1)}$ in the single input per cycle PRC $F^{(1)}(\varphi)$ and use only $F(\varphi)$, since it clearly suggests that this PRC is a single-valued function of only one stimulus phase φ.

Based on equation 2.1, a negative value of the PRC means that the next spike is advanced; otherwise it is delayed. Others (Ermentrout, 1996; Nadim, Zhao, & Bose, 2012) prefer to flip the sign in equation 2.1 and associate a positive sign to a phase advance. Often the effect of a single stimulus extends to subsequent cycles and is measured by higher-order PRCs (Oprisan, 2012a, 2012b, 2014b). Usually at least five cycles are recorded until the neural oscillatory returns to its unperturbed oscillatory activity (Oprisan et al., 2003, 2004). Afterward, another single stimulus is applied at a different phase to quantify its effect on the isolated neuron (open-loop experimental setup). As a result of the perturbation, according to equation 2.1, the new firing period becomes $P_1 = P_i(1 + F(\varphi))$, where $F(\varphi)$ represents the relative shortening or lengthening of the intrinsic firing period P_i due to the stimulus applied at phase φ (Oprisan, 2012a, 2012b, 2014b).

Figure 1b shows a typical type 1 PRC in response to a brief excitatory current perturbation that produces only phase advances (period shortening), that is, negative resetting. A type 1 PRC looks unimodal and is often associated with a class I excitable cell—one that can produce stable oscillatory activity with arbitrarily low frequency (Brown, Moehlis, & Holmes, 2004; Ermentrout, 1996). Usually such excitable cells produce stable oscillations via a saddle-node bifurcation on an invariant circle (see Izhikevich, 2000, for a detailed description of bifurcations and neural class types). It was recently shown that type 1 (unimodal) PRCs do not always come from a class I excitable cell (Ermentrout, Glass, & Oldeman, 2012), and in fact all PRCs are bimodal with varying degrees (Oprisan, 2013, 2014b). The amount of phase resetting induced by a presynaptic stimulus depends on its timing (phase) and the pre- to postsynaptic coupling strength g. For example, in the case of the excitatory coupling between neurons 2 and 3, a weak coupling of $g_{23} = 0.0175$ (arbitrary units, hereafter arb. units) produces a maximum resetting of about 25% of the intrinsic period (continuous red line). A stronger coupling of $g_{23} = 0.0275$ (arb. units) produces maximum 40% resetting (dashed green line), and an even stronger coupling of $g_{23} = 0.051$ (arb. units) induces an 80% resetting (dotted blue line). The horizontal line

$P_{1i}/P_{3i} - 1$ shows by how much the transient phase of the feedback loop neuron 3 should be reset to bring its intrinsic period P_{3i} to the common firing period of the network, which is P_{1i}. As we notice from Figure 1b, the network could possibly find a common firing rhythm only if the coupling is stronger than $g_{23} = 0.0175$ (arb. units), that is, the stimulus resets the follower neuron at least by the intrinsic period mismatch $P_{1i}/P_{3i} - 1$.

One key assumption in generalizing the PRC method to multiple inputs per cycle is that the resetting induced by one stimulus takes effect almost instantaneously, before the arrival of the next stimulus. Therefore, the effects of two stimuli applied during the same cycle are independent of each other. As a result, we recursively used the single-stimulus PRCs $F(\varphi)$ shown in Figure 1b to compute the phase resetting in response to two or more stimuli. Briefly, the first stimulus delivered at stimulus phase $\varphi_a = t_{sa}/P_i$ produced a transient change in the firing period to $P_a = P_i(1 + F(\varphi_a))$. The second stimulus that arrived at a stimulus phase $\varphi_b = t_{sb}/P_a > \varphi_a$ further resets the firing period to $P_b = P_a(1 + F(\varphi_b))$. Combining these effects of the two stimuli applied at phases φ_a and φ_b, the new firing period P_b becomes (for a detailed derivation and a generalization to n inputs per cycle, see appendix B)

$$P_b = P_i(1 + F^{(2)}(\varphi_a, \varphi_b)) = P_i(1 + F(\varphi_a))(1 + F(\varphi_b)), \tag{2.2}$$

where $F^{(2)}(\varphi_a, \varphi_b)$ is the PRC in response to two stimuli at phases φ_a and, respectively, φ_b. We again simplified the notation $F^{(2)}(\varphi_a, \varphi_b)$ by dropping the superscript $^{(2)}$ and retaining only the notation $F(\varphi_a, \varphi_b)$ for the recursive definition of the PRC given by equation 2.2.

A typical two-stimuli phase-resetting surface $F(\varphi_a, \varphi_b)$ is shown in Figure 1d, where the three-dimensional surface is given by equation 2.2, and a two-dimensional contour plot also shows the contours of equal phase-resetting. The fact that the phase-resetting surface and its two-dimensional contour projection onto (t_{sa}, t_{sb}) plane is chopped reflects the physical restriction that the second stimulus comes after the first: $t_{sb} > t_{sa}$. For this plot, we used the analytical normal form of the PRC (see equation 2.3) where $P_{2i} = 70$ ms and the coupling strength from neuron 1 to neuron 2 was $g_{12} = 0.015$ (excitatory) and from neuron 3 to neuron 2 was $g_{32} = 0.002$ (inhibitory) (see section 3 for a detailed description of the neural model and the synaptic couplings).

Close to the saddle-node bifurcation point that leads to stable oscillations, accurate analytical formulas, called normal forms, describe the single stimulus PRCs (see Brown et al., 2004, for mathematical details):

$$F(\varphi) = \frac{c_{SN}}{\omega}(1 - \cos(2\pi\varphi)), \tag{2.3}$$

where c_{SN} is a constant determined by the neural model and $\omega = 2\pi/P_i$ is the intrinsic angular frequency of the oscillator.

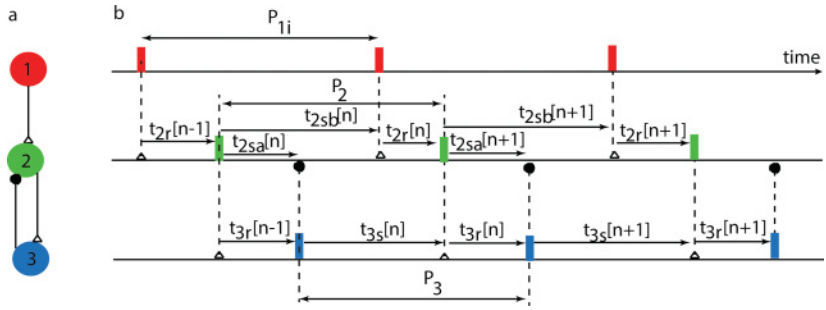

Figure 2: Typical phase-locked mode with one neuron receiving two inputs per cycle. Neuron 1 (red circle in panel a and red vertical line in panel b) with the intrinsic firing period P_{1i} is the driver of the entire network. The neural spikes are represented by thick vertical lines in panel b. The coupling between the neurons is marked by vertical dashed lines that terminate with either an excitatory (empty triangle) or an inhibitory (solid circle) synapse (panel b). Neuron 2 (green circle in panel b) receives two inputs during the same cycle. The first is an inhibition at stimulus time t_{2sa} from the interneuron 3 (blue circle in panel a); later it receives an excitatory input from neuron 1 at stimulus time t_{2sb}. Neuron 2 recovers from the last stimulus after t_{2r} and fires again. Neuron 3 receives only one excitatory input per cycle from neuron 2.

We numerically generated PRCs for each neuron of the neural network in response to a single spike from its corresponding presynaptic neuron, that is, open loop PRCs. As we notice from Figure 1b, the PRCs are determined by the strength g of the synaptic coupling according to the mathematical model in section 3. The experimentally measurable coupling strength g and the abstract coupling constant c_{SN} of the normal form PRC given by equation 2.3 represent similar quantities. However, in order to use the normal form in place of the numerically generated PRCs and vice versa, we needed to clearly establish the relationship between c_{SN} and g. For this purpose, we used least-square fitting to match the theoretical formula of the normal form PRC given by equation 2.3 with the numerically generated open loop PRCs. We found a very good match, and the normal form coupling strengths c was simply proportional to the maximum synaptic couplings g: $c_{12} = -6.1733g_{12} - 0.0003$, $c_{23} = -6.9555g_{23} - 0.0005$, and $c_{32} = 7.2764g_{32} + 0.0002$.

3 The Model

All neurons in the neural network shown in Figure 2 were implemented using Morris-Lecar (type 1) equations (see Morris & Lecar, 1981, and appendix A for mathematical details). We also implemented fast chemical

synapses between neurons (see Destexhe, Mainen, & Sejnowski, 1994; Kopell & Somers, 1993, and appendix A for mathematical details).

For neurons 2 and 3 in Figure 2, we numerically computed the PRCs in open loop setup by injecting a single synaptic input from the corresponding presynaptic neuron shown in our neural network configuration. The freeware XPPAUT (Ermentrout, 2002) can compute the single stimulus PRC for any given model equations.

3.1 The Neural Network Model. In order to use the phase-resetting method (see section 2) for predicting the relative phases of neurons in a phase-locked firing pattern, we assumed a fixed firing order of the three neurons with the goal of determining if such a pattern exists (see section 4) and if it is stable (see section 5). Using the neural network model proposed for delayed and anticipated synchronization by (Matias et al., 2011, 2014, 2015; Matias, 2014) we identified the following definitions for the firing periods of the three neurons (see Figure 2):

$$\begin{aligned} P_1 &= t_{2r}[n-1] + t_{2sb}[n], \\ P_2 &= t_{2sb}[n] + t_{2r}[n], \\ P_3 &= t_{2sb}[n] - t_{2sa}[n] + t_{2r}[n] + t_{2sa}[n+1], \end{aligned} \tag{3.1}$$

where t_{2r} is the recovery time of neuron 2 after its last inputs, t_{2sa} and t_{2sb}, are the corresponding stimulus times for the first and, respectively, the second input to neuron 2, and the index of the cycle is marked with the square brackets $[\ldots]$. The subscript index refers to the neural oscillator index according to Figure 2. Since neuron 1 received no feedback from any other neuron, its firing period is constant, $P_1 = P_{1i}$. We eliminated $t_{2r}[n-1] = P_{1i} - t_{2sb}[n]$ from equations 3.1 and substituted it into the other two equations, which led to

$$\begin{aligned} P_2 &= t_{2sb}[n] + P_{1i} - t_{2sb}[n+1], \\ P_3 &= t_{2sb}[n] - t_{2sa}[n] + P_{1i} - t_{2sb}[n+1] + t_{2sa}[n+1]. \end{aligned} \tag{3.2}$$

Based on the definitions of the PRCs (see equations 2.1 and 2.2), we further expanded equations 3.2 representing the transiently modified firing periods in terms of single-stimulus PRCs:

$$\begin{aligned} P_{2i}(1 + F_2(t_{2sa}[n], t_{2sb}[n])) &= t_{2sb}[n] + P_{1i} - t_{2sb}[n+1], \\ P_{3i}(1 + F_3(t_{s3}[n])) &= t_{2sb}[n] - t_{2sa}[n] + P_{1i} - t_{2sb}[n+1] \\ &\quad + t_{2sa}[n+1]. \end{aligned} \tag{3.3}$$

Here and throughout the rest of the letter, we used another simplified notation where the stimulus time and the corresponding stimulus phase were

interchangeable. For example, we write $F_3(t_{s3})$ with the understanding that we referred here to the phase-resetting of neuron 3 calculated according to the definition given by equation 2.1 at its corresponding phase $\varphi_3 = t_{3s}/P_{3i.}$ This simplification of notation allows us to naturally move between the existence conditions for phase-locked modes, such as equations 3.3, that are more conveniently written in terms of time (instead of phase) and the stability conditions (see section 5) that are more conveniently expressed in terms of phase.

The above system of two recursive equations has two unknowns, t_{2sa} and t_{2sb}, that describe the temporal evolution of the relative phase of neural oscillators from the firing cycle $[n]$ to $[n+1]$.

4 Results: The Existence of Phase-Locked Modes

Let us assume that the recursive equations 3.3 that mimic the activity of the neural network shown in Figure 2 have the steady-state solution (t^*_{2sa}, t^*_{2sb}). By substituting the steady-state (i.e., phase-locked mode) solution (t^*_{2sa}, t^*_{2sb}) into equation 3.3, one obtains

$$\begin{aligned} P_{2i}(1 + F_2(t^*_{2sa}, t^*_{2sb})) &= P_{1i}, \\ P_{3i}(1 + F_3(P_{1i} - t^*_{2sa})) &= P_{1i}, \end{aligned} \tag{4.1}$$

where we used the fact that $t^*_{3s} = t^*_{2sb} - t^*_{2sa} + t^*_{2r}$ and that $t_{2r}[n-1] = P_{1i} - t_{2sb}[n]$, which led to $t^*_{3s} = t^*_{2sb} - t^*_{2sa} + P_{1i} - t^*_{2sb} = P_{1i} - t^*_{2sa}$.

From equation 4.1, it results that the steady-state value t^*_{2sa} depends on only P_{1i}, P_{3i}, and the PRC of neuron 3, which depends on the coupling strength g_{23}. Therefore, the steady-state value t^*_{2sa} is the solution of

$$F_3(P_{1i} - t^*_{2sa}) = \frac{P_{1i}}{P_{3i}} - 1. \tag{4.2}$$

In Figure 1b we show the ratio $P_{1i}/P_{3i} - 1$ with a horizontal continuous line. A steady-state t^*_{2sa} exists only at the crossing of this horizontal line with the corresponding PRC F_3. At the very minimum, the coupling strength g_{23} must ensure at least one solution (see the continuous red line PRC in Figure 1b). Below $g_{23} = 0.0175$ (arb. units) presynaptic neuron 2 cannot bring the firing period of postsynaptic neuron 3 to their common firing period of the driving neuron P_{1i}, and there is no phase-locked solution. For coupling strengths larger than the minimum required for entrainment, there are two possible steady-states t^*_{2sa} (see the two crossings of the horizontal line $P_{1i}/P_{3i} - 1$ with dashed green and dotted blue PRCs in Figure 1b). Of the two possible steady states, we will see (see section 5) that only one is stable.

Since in this study we kept all intrinsic periods constant and varied only the three coupling strengths, the parameter space is three-dimensional.

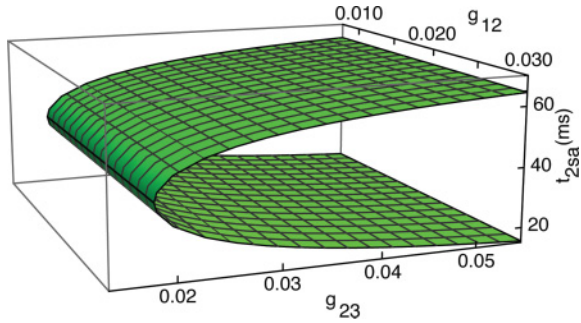

Figure 3: Steady-state surface for t^*_{2sa}. Regardless the values of g_{12}, the steady state t^*_{2sa} depends on only the coupling strength g_{23} for a fixed $g_{32} = 0.002$ arb. units. For a weak coupling of $g_{23} = 0.0175$ (see Figure 1b), there is only one solution possible, which is the cusp of the two surfaces shown here. As the coupling strength g_{23} increases, the two possible steady-state solutions for t^*_{2sa} move farther apart. Only one of the two solutions is stable (see section 5).

In some cases, such as the excitatory coupling from neuron 2 to neuron 3 that determines t^*_{2sa}, the parameter space is one-dimensional since the steady state (phase-locked mode) depends on only parameter (g_{23}). However, to simplify subsequent comparisons with other steady states (e.g., t^*_{2sb}), we presented the phase-locked mode t^*_{2sa} in a two-dimensional space of control parameters (g_{12}, g_{23}), even though g_{12} does not influence the solution t^*_{2sa}, for a constant value of the inhibitory feedback g_{32} (in Figure 3, $g_{32} = 0.002$ arb. units).

Since the coupling from neuron 2 to neuron 3 is excitatory, the PRC is negative (it only advances the next spike): $F_3(\varphi) < 0$. As a result of equation 4.2, the steady-states t^*_{2sa} can exist only for $P_{1i} < P_{3i}$, which means that the interneuron (neuron 3) must be slower than the driver (neuron 1) of the network. Moreover, since a type 1 PRC in response to excitatory inputs has only one negative minimum ($F_{3,\min}$) that determines the magnitude of the strongest possible resetting, then $\frac{P_{1i}}{P_{3i}} - 1 \geq F_{3,\min}$, which means that the interneuron's intrinsic period is bounded by $P_{1i} < P_{3i} < P_{1i}/(1 + F_{3,\min})$. Indeed, as shown in Figures 1b and 3, a too weak coupling gives a PRC that never crosses the required resetting line $P_{3i}/P_{1i} - 1$ to bring neuron 3 to the common firing period P_{1i} of the network.

Once we determined the steady-state t^*_{2sa} from equation 4.2, we plugged it into the first of equations 4.1 and found t^*_{2sb}. Using the single-stimulus PRC definition (see equation 2.2) we obtained

$$P_{2i}\alpha\left(1 + F_2\left(\frac{t^*_{2sb}}{\alpha}\right)\right) = P_{1i}, \tag{4.3}$$

where $\alpha = 1 + F_2(t^*_{2sa})$. The above equation can be reduced to

$$F_2\left(\frac{t^*_{2sb}}{\alpha}\right) = \frac{P_{1i}}{P_{2i}\alpha} - 1, \tag{4.4}$$

which has a similar geometrical interpretation with the existence criterion for t^*_{2sa} (see Figure 1b); t^*_{2sb} is the (stable) solution at the crossing of the horizontal line $P_{1i}/(\alpha P_{2i}) - 1$ and the single stimulus PRC of neuron 2. We emphasize that $F_2(t^*_{2sa})$ and $F_2(t^*_{2sb})$ are two different single-stimulus PRCs for the same neuron 2. Here, $F_2(t^*_{2sa})$ is the single-stimulus PRC of neuron 2 to an input received from neuron 3, that is, $F_2(t^*_{2sa})$ is determined by g_{32}. Similarly, $F_2(t^*_{2sb})$ is the single-stimulus phase response curve of neuron 2 in response to an input received from neuron 1, that is, $F_2(t^*_{2sb})$ is determined by g_{12}.

4.1 Explicit Steady-State Solutions Using Normal Form Generic Type 1 PRCs. In order to gain insight into the general existence criteria for the steady state (phase-locked modes) derived above, we assumed that the single-stimulus PRCs are well approximated by the normal form given by equation 2.3. Thus, the steady-state solution t^*_{2sa} of equation 4.2 can be analytically written as

$$\cos\left(2\pi\left(\frac{P_{1i}}{P_{3i}} - \frac{t^*_{2sa}}{P_{3i}}\right)\right) = 1 - \frac{1}{c_{23}P_{3i}}\left(\frac{P_{1i}}{P_{3i}} - 1\right). \tag{4.5}$$

By least-square-fitting the numerically generated PRCs for each neuron in response to a single spike from its corresponding presynaptic neuron (open loop setup) with the theoretical formula of the normal form given by equation 2.3, we found a quantitative relationship between the abstract coupling strength coefficient c and the physiologically measurable maximum synaptic couplings g. Therefore, in order to simplify the mathematical notation, throughout the rest of the letter, we only write, for example, c_{23} when referring to the coefficient of the theoretical normal form of the PRC, with the understanding that it is a known function of the corresponding synaptic conductance: $c_{23} = c_{23}(g_{23})$.

Since $-1 \le \cos(x) \le 1$, it results that $0 \le \frac{1}{c_{23}(g_{23})P_{3i}}\left(\frac{P_{1i}}{P_{3i}} - 1\right) \le 2$, which determines the minimum coupling strength g_{23} for a given ratio of the two intrinsic firing periods $\frac{P_{1i}}{P_{3i}}$ to attain a phase-locked mode pattern (see Figure 1b). Based on the above relationship, for excitatory coupling, $E_{syn} = 0$, the driving (pacemaker) neuron 1 (see Figure 2) must be faster than the interneuron 3: $P_{1i} < P_{3i}$. At the same time, the coupling strength g_{23} must also be strong enough to reset the longer intrinsic period P_{3i} to match the shorter period of the network's pacemaker: to ensure that $P_{3i} < P_{1i}/(1 + F^{(1)}_{3,\min})$.

The phase-locked modes (t^*_{2sa}, t^*_{2sb}) given by equations 3.3 depend on the three fixed intrinsic periods P_{1i}, P_{2i}, P_{3i} and the three synaptic conductances

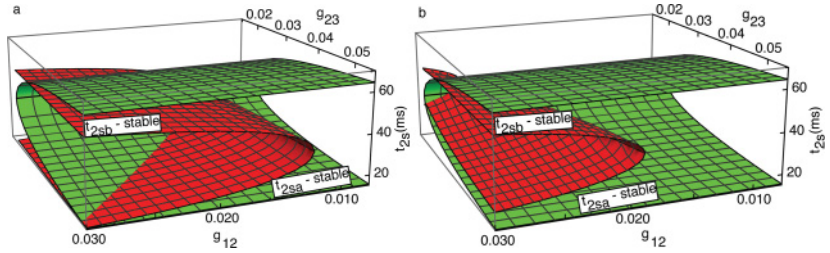

Figure 4: Steady-state firing patterns (t^*_{2sa}, t^*_{2sb}). (a) For a weak inhibition from neuron 3 to neuron 2 ($g_{32} = 0.002$ arb. units), the lengthening of the firing period of neuron 2 is not too large and can be easily compensated by a second, excitatory, input from neuron 1 with a coupling strength as low as $g_{12} = 0.01$. (b) For a much stronger inhibition ($g_{32} = 0.02$ arb. units), the lengthening of neuron 2's period is much larger; it requires a stronger excitatory coupling with a minimum strength of $g_{12} = 0.02$ in order to bring its period to the common value of P_{1i}.

g_{12}, g_{23}, and g_{32}. Intuitively, the phase-locked solution t^*_{2sa} is the stable interspike interval between neurons 2 (the driven neuron) and 3 (the interneuron). The other phase-locked solution t^*_{2sb} is the stable interspike interval between neurons 2 and 1 (the network's driver).

In order to further reduce the parameter space, we plotted three-dimensional steady-state surfaces for a fixed value of the only inhibitory coupling g_{32}. The solution t^*_{2sa} of the second equation in equations 3.3 depends on only the coupling strength g_{23} (see the green surface in Figures 3 and 4). However, the phase-locked solution t^*_{2sb} of the first equation in equations 3.3 depend on the additional coupling g_{12}. Therefore, to gain insight into how the steady state (t^*_{2sa}, t^*_{2sb}) of the network shown in Figure 2 depends on the excitatory couplings g_{12} and g_{23} for a fixed value of g_{32}, we plotted them together in Figure 4. Of the two possible steady-state solutions for t^*_{2sa}, only the lower green surface (marked "t_{2sa} - stable" in Figure 4) corresponds to an actual, (i.e. stable; see section 5) phase-locked pattern. Similarly, of the two possible steady-state solutions for t^*_{2sb}, only the upper red surface (marked "t_{2sb} - stable" in Figure 4) corresponds to an actual phase-locked pattern. As the inhibitory synaptic strength g_{32} becomes stronger (from $g_{32} = 0.002$ in Figure 4a to $g_{32} = 0.02$ in Figure 4b), the excitatory coupling g_{12} from driving neuron 1 must be stronger. This is because a stronger inhibition of neuron 2 by neuron 3 (larger g_{23}) means that the transiently modified firing period of neuron 2 becomes larger and larger. However, for a phase-locked mode to exist, the firing period of all neurons must match the intrinsic period P_{1i} of the driving neuron (which is the shortest of all three neurons). As a result, the second, excitatory, stimulus that neuron 2 receives from neuron 1 must compensate for a longer period

induced by a previous inhibition, which requires a stronger excitatory coupling g_{12}.

5 The Stability of Phase-Locked Modes

The possible phase-locked modes given by equations 3.3 may not all be stable and therefore may not be all observable. To determine the stability of the steady solutions (t^*_{2sa}, t^*_{2sb}), we assume small perturbations:

$$\begin{aligned} t_{2sa}[n] &= t^*_{2sa} + \delta t_{2sa}[n], \\ t_{2sb}[n] &= t^*_{2sb} + \delta t_{2sb}[n], \end{aligned} \tag{5.1}$$

where the n^{th} cycle perturbation $\delta t_{2s}[n] \ll t^*_{2s}$ is assumed very small for both stimuli. By substituting equations 5.1 into the existence criteria from equations 4.1 and using a Taylor series expansion, one obtains

$$\begin{aligned} m_{2a}(1+F_2(\varphi^*_{2b})-\varphi^*_{2b})\delta t_{2sa}[n]+m_{2b}\delta t_{2sb}[n] &= \delta t_{2sb}[n] - \delta t_{2sb}[n+1], \\ m_3(\delta t_{2sb}[n] - \delta t_{2sa}[n] - \delta t_{2sb}[n+1]) &= \delta t_{2sb}[n] - \delta t_{2sa}[n] \\ &\quad - \delta t_{2sb}[n+1]+\delta t_{2sa}[n+1], \end{aligned} \tag{5.2}$$

where $m_{2a} = \left(\frac{\partial F_2}{\partial \varphi}\right)_{\varphi^*_{2a}}$ is the slope of the second neuron's PRC at the phase of the first stimulus $\varphi^*_{2a} = \frac{t^*_{s2a}}{P_{2i}}$, $m_{2b} = \left(\frac{\partial F_2}{\partial \varphi}\right)_{\varphi^*_{2b}}$ is the slope of the second neuron's PRC at the phase of the second stimulus $\varphi^*_{2b} = \frac{t^*_{s2b}}{P_{2i}(1+F_2(t^*_{2sa}))}$, and $m_3 = \left(\frac{\partial F_3}{\partial \varphi}\right)_{\varphi^*_3}$ is the slope of the third neuron's PRC at the phase of the stimulus $\varphi^*_2 = \frac{t^*_{s3}}{P_{3i}}$. The stability equations 5.2 can be rewritten in a matrix form as a first-order recursive relationship for the perturbations:

$$\begin{pmatrix} \delta t_{s2a} \\ \delta t_{s2b} \end{pmatrix}_{[n+1]} = \begin{pmatrix} a_{11} & a_{12} \\ a_{21} & a_{22} \end{pmatrix} \begin{pmatrix} \delta t_{s2a} \\ \delta t_{s2b} \end{pmatrix}_{[n]}, \tag{5.3}$$

where $a_{11} = (1-m_3)(1-b)$, $a_{12} = -(1-m_3)m_{2b}$, $a_{b2} = -b$, and $a_{22} = 1 - m_{2b}$ with $b = m_{2a}(1+F_2^{(1)}(\varphi^*_{2b}) - m_{2b}\varphi^*_{2b})$. The stability of the steady state is determined by the eigenvalues of equation 5.3. Briefly, the trace $Tr(A) = a_{11} + a_{22}$ and the determinant $Det(A) = a_{11}a_{22} - a_{12}a_{21}$ of the recursion matrix in equation 5.3 determine the stability of each steady state obtained by solving the characteristic polynomial $\lambda^2 - (TrA)\lambda + DetA = 0$. For a steady state to be stable, both eigenvalues must be less than unit: $|\lambda_{1,2}| < 1$.

In Figure 5 we plot the two eigenvalues (λ_1 in panels a and b, and λ_2 in panels c and d) for a weak inhibition of $g_{32} = 0.002$ (panels a and c) and for stronger inhibition of $g_{32} = 0.02$ (panels b and d). Both Figures 4 (steady

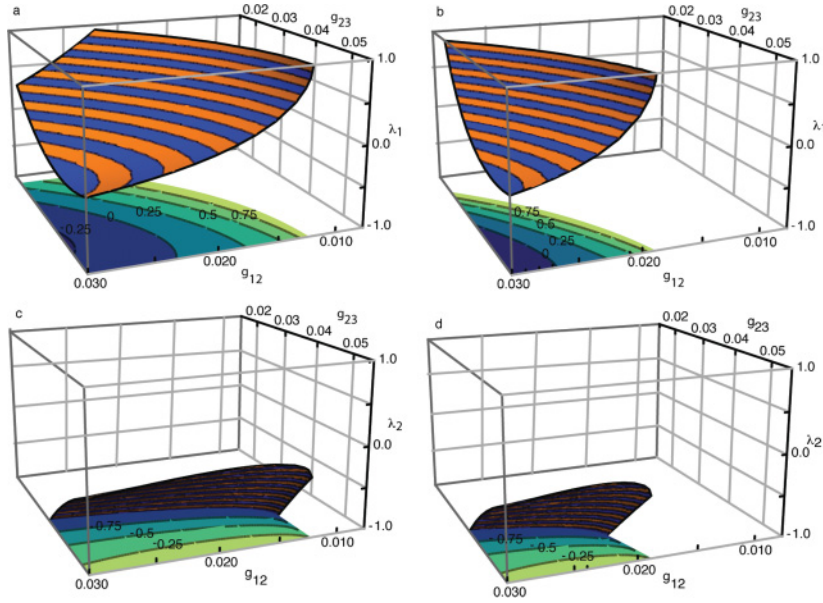

Figure 5: The eigenvalues determine the stability of steady state. For a fixed and weak inhibitory coupling of $g_{32} = 0.002$ arb. units, the eigenvalues λ_1 (a, b) and λ_2 (c, d) determine the range of coupling strengths (g_{12}, g_{23}) that give stable phase-locked modes. If the inhibitory coupling strength increases by one order of magnitude (panels b, respectively, d), then the excitatory coupling g_{12} must also increase while it has little effect on g_{23}.

states) and 5 (stability of steady states) have the same axes and the same three-dimensional viewpoint to facilitate comparison. Each eigenvalue limits the range of one synaptic coupling. For example, λ_1 (see Figure 5a) covers a wide range of g_{23} values but requires a minimum coupling of $g_{12} \approx 0.012$ arb.units. At the same time, λ_2 (see Figure 5c) covers the entire range of $g_{12} > 0.012$ but requires a minimum coupling of $g_{23} \approx 0.027$ arb. units. As the inhibitory coupling strength increases to $g_{32} = 0.02$ arb. units, we need a stronger excitatory input from the driving neuron g_{12} (see Figure 5b and the previous discussion in section 4). The stability condition for λ_2 (see Figure 5d) shows that increasing the inhibitory coupling strength g_{32} by an order of magnitude has little to no effect on the required range of excitatory coupling g_{23}.

The original recursive system given by equations 3.1 contained three variables, which were reduced to two coupled recursive equations (see equations 3.2) by eliminating the third variable, $t_{2r}[n-1] = P_{1i} - t_{2sb}[n]$. As a result, the third steady-state solution is $t^*_{2r} = P_{1i} - t^*_{2sb}$, and the corresponding infinitesimal perturbation is $\delta t_{2r}[n-1] = -\delta t_{2sb}[n]$. Therefore, the

stability of third steady-state solution t^*_{2r} is determined by the stability of $\delta t_{2sb}[n]$, which was already covered by equation 5.3.

6 Numerical Validation of the Existence and the Stability Criteria

The analytically derived criteria for the existence (see section 4) and stability (see section 5) of phase-locked modes in a driving-driven network with a dynamic loop (see Figure 2) were based on the generalized PRC, that is, the recursive relationships involving single stimulus PRCs. We checked our theoretical predictions based on open loop PRCs against numerical simulations of the actual neural networks implemented according to the model presented in section 3: closed loop (fully connected neural network).

The analytical normal form PRC formulas (see equation 2.3) were convenient analytical tools and even led us to some analytical results in the preceding sections. However, for the actual comparison between the multiple stimuli PRC-based phase-locked mode prediction (open loop) and the numerical simulations results of the fully coupled neural network (see Figure 2), we used numerically generated open loop PRCs. The reason is that although the analytical normal form of type 1 PRC given by equation 2.3 is close to the numerically generated open loop PRC (not shown), we wanted a more accurate prediction based on the real-world PRC as it would be generated in wet lab/numerical experiments. A Mathematica file that contains the implementation of the neural network shown in Figure 2 based on the model equations provided in the online section 3 is available in the online supplement.

The synaptic couplings used for the example shown in Figure 6a were $g_{12} = 0.015$, $g_{32} = 0.002$, and $g_{23} = 0.0275$, which led to a phase-locked mode with $t^*_{2sa} = 15.2$ ms and $t^*_{2sb} = 40.2$ ms. The PRC-based predictions were $t^*_{2sa} = 18.0$ ms (about 18% error) and $t^*_{2sb} = 44.1$ ms (about 10% error). We found that the eigenvalues of the stability matrix were $\lambda_1 = 0.489$ and $\lambda_2 = 0.779$, which indicated that the predicted mode was stable. Figure 6b shows a similar firing pattern with a much stronger inhibitory feedback of $g_{32} = 0.02$ arb. units and a corresponding stronger excitatory coupling of $g_{12} = 0.04$ arb. units (with $g_{23} = 0.0275$), which led to a phase-locked mode with $t^*_{2sa} = 15.2$ ms and $t^*_{2sb} = 50.3$ ms. The PRC-based predictions were $t^*_{2sa} = 17.0$ ms (about 11% error) and $t^*_{2sb} = 49.0$ ms (about 3% error). We found that the eigenvalues of the stability matrix were $\lambda_1 = 0.488$ and $\lambda_2 = -0.314$, which indicated that the predicted mode was stable.

7 Discussion

There are two novelties in this study: (1) a generalized, recursive definition of the PRC in response to multiple inputs per cycle that was applied to (2) a biologically relevant three-neuron network.

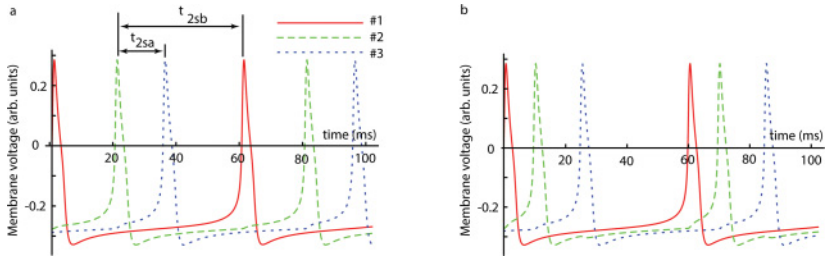

Figure 6: Phase-locked modes in fully coupled neural network. (a) A typical stable phase-locked mode in which neuron 2 (dashed line) receives two inputs during a single cycle: first from neuron 3 (dotted line) at t^*_{2sa} and then from neuron 1 (solid line) at t^*_{2sb}. The experimental values for the phase-locked mode as measured from panel b were $t^*_{2sa} = 15.2$ ms and $t^*_{2sb} = 40.2$ ms, whereas the PRC-based predictions were $t^*_{2sa} = 18.0$ ms and $t^*_{2sb} = 44.1$ ms. The network's firing period was $P = 60$ ms $= P_{1i}$. The synaptic couplings were $g_{12} = 0.015$, $g_{23} = 0.0275$, and $g_{32} = 0.002$ arb. units. (b) A similar firing pattern for an inhibitory coupling one order of magnitude stronger: $g_{32} = 0.02$ arb. units.

We previously applied the PRC method to predicting phase-locked modes in three-neuron networks with ring topology (see Oprisan & Canavier, 2002a, 2002b). The ring network topology ensured that each neuron received only one input per cycle; hence we were able to use the single-stimulus PRC as defined since the early 1960s (see Perkel et al., 1964). Despite this limitation due to the particular ring topology, in Oprisan and Canavier (2002a, 2002b), we addressed two important issues: (1) the contribution of the second-order PRC and (2) the effect of long pulses (as opposed to infinitesimally short perturbations that are usually used for generating PRC).

In order to generalize the PRC to multiple inputs per cycle, we first investigated the fundamentals of how the single-stimulus PRC is actually generated by exploring the effect of external stimuli on the phase-space trajectory of figurative points (see Oprisan & Canavier, 2002a, 2002b). Using phase-space analysis, we successfully predicted analytically the shape of single-stimulus PRC for type 1 oscillators. However, the most significant contribution of the Oprisan and Canavier (2002a, 2002b) study was the theoretical formula of the PRC in response to two stimuli (see section 3.2, "Phase Resetting Induced in a Type 1 Oscillator by Multiple Inputs per Cycle"). Our first attempt to produce a theoretical prediction for the PRC in response to two inputs per cycle as shown by equation 3.4 of Oprisan and Canavier (2002a, 2002b) assumed a linear combination for the effects of the two stimuli:

$$F^2(\varphi) = F^1(\varphi) + F^1(\varphi + F^1(\varphi) + (t_2 - t_1)/P_i), \tag{7.1}$$

where t_1 and t_2 were the stimulus times.

Based on subsequent studies, we now know that the linear approximation given by equation 7.1 does not entirely capture the intrinsically nonlinear nature of neural processing of multiple inputs. However, for type 1 neural oscillators with infinitely attractive limit cycles, the prediction of phase-locked modes given by equation 7.1 was quite satisfactory when compared against the experiments (see Figure 10 in Oprisan and Canavier, 2002a, 2002b, and Oprisan, 2012b).

We subsequently used the theoretical PRC in response to multiple inputs per cycle derived in Oprisan and Canavier (2002a, 2002b) as shown in equation 7.1 to predict the phase-locked modes in neural networks with a neuron driven by two stimuli applied during the same cycle (see Figure 1 in Oprisan & Canavier, 2003) for network architecture).

Although our linear approximation of the PRC for two inputs per cycle derived in Oprisan and Canavier (2002a, 2002b; see equation 7.1 above) gave very good results for type 1 neural oscillators, we were also aware that it was significantly off in predicting the PRC for type 2 oscillators. We recently revisited the phase-space method and successfully incorporated both the tangent perturbations to limit cycle, the hallmark of type 1 oscillators, and the normal perturbations, which is the signature of type 2 oscillators (Oprisan, 2014a).

With the results derived in Oprisan (2014a), it became obvious why the linear recursive PRC initially derived in Oprisan and Canavier (2002a, 2002b) (see equation 7.1 above) worked perfectly only for type 1 neural oscillators and how it should be generalized to also describe type 2 oscillators, which we did in Vollmer et al. (2015) and expanded in this study.

8 Conclusion

Since even for this small unidirectionally coupled three-neuron network, the parameter space is six-dimensional—three intrinsic firing periods (P_{1i}, P_{2i}, and P_{3i}), one unidirectional synaptic coupling between driving-driven neurons (g_{12}), and two coupling constants for the feedback loop (g_{23} and g_{32})—we reduced it to manageable dimensions in order to visualize the phase-locked solution. Since the driving neuron receives no feedback from the network, its intrinsic firing period P_{1i} was considered the reference duration, which reduces the parameter space to five dimensions. We further reduced the parameter space to three dimensions by keeping all intrinsic firing periods constant.

We numerically found the phase-locked modes (t^*_{2sa}, t^*_{2sb}) by considering two separate cases: a weak inhibitory feedback of $g_{32} = 0.002$ arb. units and a stronger inhibitory feedback of $g_{32} = 0.02$ arb. units. In all numerical simulations, the other two free parameters were the excitatory couplings (g_{12}, g_{23}). The reason we used g_{32} as a coarse control parameter is that it was previously shown that the interneuron through its intrinsic properties and its synaptic coupling can lead to either delayed or anticipating

synchronization in this neural network (Matias, 2014; Matias et al., 2014, 2015), and our goal was to closely match previous findings using the newly developed generalized PRC method.

Based on Figure 4a, increasing the strength of the driving-driven synaptic coupling g_{12} leads to a larger phase difference between the two steady states t^*_{2sa} and t^*_{2sb}. As the inhibitory coupling becomes stronger (see Figure 4b), the parameter space of the steady state shifts toward stronger excitatory couplings g_{12}. At the same time, while a stronger inhibition g_{32} requires a stronger excitatory coupling g_{12} (see Figure 4b), it seems that the excitatory coupling g_{23} becomes less critical to the stability of the phase-locked mode and gains a broader range compared to Figure 4a. Indeed, from Figure 4a, it seems that a stronger excitatory coupling g_{12} requires a stronger excitatory coupling g_{23} to the interneuron. All-out numerical simulations are in agreement with previously observed firing patterns in this type of neural network (Matias, 2014; Matias et al., 2014, 2015).

We used a generalized phase-resetting method to predict the existence and the stability of phase-locked modes in a driving-driven network with a dynamic feedback loop. This study brings two novel solutions to phase-locked mode prediction in neural networks. First, we generalized the phase response curve definition to include the more realistic case when neural oscillators receive more than one input per cycle. Second, we applied the generalized phase-resetting definition to a biologically relevant neural network that has been shown to produce both delayed and anticipated synchronization.

Predicting phase-locked modes in large neural networks usually requires as a first step a complexity reduction to manageable subnetworks of two neurons (Skinner, Bazzazi, & Campbell, 2005; Netoff, Acker, Bettencourt, & White, 2005) or, whenever possible, reduces the entire network to a two-population network (Pervouchine et al., 2006). Our PRC generalization to multiple inputs per cycle is a significant advance in phase-resetting theory that allows investigation of large networks in which individual neurons receive multiple inputs per cycle without assuming special network connectivity. Furthermore, our generalization of the phase-resetting curve and the detailed procedure we presented for predicting the existence and the stability of phase-locked modes in a biologically relevant three-neuron network with a dynamic feedback loop is not limited to weak coupling or one-to-one firing patterns. Indeed, the coupling strengths used were quite large, such that it resets the firing period of interneuron 3 by 25% from 80 ms to 60 ms.

We also carried out a detailed numerical analysis of the stability domain for the predicted phase-locked modes. In the parameter space of the three conductances (g_{12}, g_{23}, g_{32}), we found that the inhibitory feedback g_{32} from the interneuron and the excitatory input g_{12} from the driving neuron determine the phase difference between the neurons. Moreover, to produce a stable phase-locked mode, it seems that the two synaptic couplings must be

proportional to each other, such that the period lengthening produced by the inhibitory input is compensated by the period shortening induced by a later excitation.

Appendix A: Computational Model

In all our numerical simulations, we used a single-compartment Morris and Lecar (ML) mathematical model (Morris & Lecar, 1981),

$$\begin{aligned} dV/dt &= -\bar{g}_{Ca}m(V)(V - E_{Ca}) - \bar{g}_K w(V - E_K) - \bar{g}_{Leak}(V - E_{Leak}) + I_0, \\ dw/dt &= \phi(w_\infty(V) - w)/\tau(V), \end{aligned} \tag{A.1}$$

where V is the membrane potential, $\bar{g}_{ch}$ and E_{ch} are the maximum conductance and, respectively, the reversal potential for ionic channel ch (only calcium, potassium and leak were considered), w is the instantaneous probability that a potassium channel is open, and I_0 is a constant bias current, ϕ is a temperature-dependent parameter, and a voltage-dependent relaxation time constant is defined by $\tau(V) = \cosh^{-1}((V - V_{w,1/2})/(2V_{w,slope}))$. All open-state probability functions, or steady-state gating variables x, have a sigmoidal form (Morris and Lecar, 1981):

$$x(V) = (1 + \tanh((V - V_{x,1/2})/V_{x,slope}))/2, \tag{A.2}$$

where $V_{x,1/2}$ is the half-activation voltage and $V_{x,slope}$ is the slope factor for the gating variable x. The ML model is widely used in computational neuroscience because it captures relevant biological processes and, at the same time, by changing only a small subset of parameters, it can behave as either a type 1 or type 2 neural oscillator. The dimensionless parameters for a type 1 ML neuron are $V_{m,1/2} = -0.01$, $V_{m,slope} = 0.15$, $V_{w,1/2} = 0.1$, $V_{w,slope} = 0.145$, $V_K = -0.7$, $V_{Leak} = -0.5$, $V_{Ca} = 1.0$, $\bar{g}_{Ca} = 1.33$, $\bar{g}_K = 2.0$, $\bar{g}_{Leak} = 0.5$, $I_0 = 0.070$, and $\phi = 0.6$ (Ermentrout, 1996). The model's equations and its parameters are in dimensionless form with all voltages divided by the calcium reversal potential $V_{Ca0} = 120$ mV, all conductances divided by $\bar{g}_{Ca0} = 4$ mS/cm^2, and all currents normalized by $V_{Ca0}\bar{g}_{Ca0} = 480\mu$A/cm^2 (Ermentrout, 1996). For example, a dimensionless reversal potential for a leak current of $V_{Leak} = -0.5$ means $V_{Leak} = -0.5V_{Ca0} = -0.5 \times 120$ mV $= -60$ mV.

A.1 The Synaptic Model. We implemented fast chemical synapses between neurons given by a synaptic current $I_{syn} = \bar{g}_{syn}s(t)(V_{post} - E_{syn})$, where $\bar{g}_{syn}$ is the maximum synaptic conductance, $s(t)$ is the fraction of channels activated by neurotransmitters, V_{post} is the membrane potential of the postsynaptic neuron, and E_{syn} is the reversal potential of the synaptic coupling. We used $E_{syn} = 0$ for excitatory and $E_{syn} = -0.6$ for inhibitory coupling. The synapses' activation was described by a first-order kinetics

$s' = \alpha T(1-s) - \beta s$, where $\alpha = 15$, $\beta = 1.5$, and neurotransmitter binding was described by a sigmoidal function $T(V_{pre}) = 1/(1 + e^{(-V_{pre}-0.2)120/5)})$ where V_{pre} is the membrane potential of the presynaptic neuron (Destexhe et al., 1994; Kopell & Somers, 1993).

Appendix B: Phase Resetting in Response to Multiple Stimuli

Assuming that the resetting induced by one stimulus takes effect almost instantaneously (i.e., before the arrival of the second stimulus), then the effects of two stimuli applied during the same cycle are independent of each other, and we could use the single-stimulus PRC defined by equation 2.1 (shown in Figures 1c and 1d) to compute the phase resetting in response to two or more stimuli. In order to compute the phase resetting induced by the second stimulus based on equation 2.1, we need to correctly compute its phase (see Figure 2a). The phase of the first stimulus that arrives at a stimulus time t_{sa} is $\varphi_a = t_{sa}/P_i$. The first stimulus produces almost instantaneously phase resetting and changes the firing period to

$$P_a = P_i(1 + F(\varphi_a)) = P_i\left(1 + F\left(\frac{t_a}{P_i}\right)\right). \tag{B.1}$$

When the second stimulus arrives at a stimulus time $t_{sb} > t_{sa}$, the neuron already has a different firing period P_a due to the previous stimulus. As a result, the phase of the second stimulus is $\varphi_b = t_{sb}/P_a$ and the new firing period due to the second stimulus is:

$$P_b = P_a(1 + F(\varphi_b)) = P_a\left(1 + F\left(\frac{t_b}{P_a}\right)\right), \tag{B.2}$$

where we used the same definition of the first-order phase resetting for a single stimulus as in equation 2.1. By substituting equation B.2 into equation B.3 one obtains:

$$\begin{aligned} P_b &= P_a(1 + F(\varphi_b)) \\ &= P_i\left(1 + F\left(\frac{t_a}{P_i}\right)\right)\left(1 + F^{(1)}\left(\frac{t_b}{P_i\left(1 + F\left(\frac{t_a}{P_i}\right)\right)}\right)\right), \end{aligned} \tag{B.3}$$

which could be rewritten to resemble equation 2.1:

$$P_b = P_i(1 + F(\varphi_a, \varphi_b)), \tag{B.4}$$

where the notation $F(\varphi_a, \varphi_b)$ clearly emphasizes that the new transient period P_b is computed in response to two stimuli arriving at phases φ_a and,

respectively, $\varphi_b > \varphi_a$ during the same cycle. By comparing the definition from equation B.4 against the derived resetting from equation B.3, we found that

$$F(t_{sa}, t_{sb}) = \left(1 + F\left(\frac{t_a}{P_i}\right)\right)\left(1 + F\left(\frac{t_b}{P_i\left(1 + F\left(\frac{t_a}{P_i}\right)\right)}\right)\right) - 1, \tag{B.5}$$

which has the advantage that it can predict the phase resetting in response to two stimuli by recursively using the single-stimulus PRC defined in equation 2.1. A typical two-stimuli-phase resetting surface is shown in Figure 2b.

Furthermore, our novel derivation of PRC in response to two stimuli given by equation B.5 generalizes to an arbitrary number of inputs per cycle as follows:

$$P_n(t_{s1}, t_{s2}, \ldots, t_{sn}) = P_i \prod_{k=1}^{n}\left(1 + F\left(\frac{t_{sk}}{P_{k-1}}\right)\right), \tag{B.6}$$

where $P_0 = P_i$ is the intrinsic firing period of the isolated neuron, P_n is the transiently modified period of that neuron after n successive stimuli applied during the same cycle, $t_{sk} > t_{s(k+1)}$, and $t_{sk} < P_{k-1}$—the k^{th} stimulus falls inside the transiently modified period P_{k-1} due to the previous stimulus.

Acknowledgments

We are grateful to Mauro Copelli and Claudio R. Mirasso for suggesting to us this important and biologically relevant three-neuron neural network. We are grateful to anonymous reviewers for drawing our attention to other biologically relevant three-neuron networks, such as the generic Fitzhugh-Nagumo network with reciprocal couplings (Schwabedal et al., 2016) and the building block motif of the central pattern generator network controlling swim locomotion of sea slug *Melibe leonina* (Alacam & Shilnikov, 2015), which could potentially use the theoretical method described in this manuscript.

This research was supported by the U.S. National Science Foundation Career Award IOS 1045914 to SAO.

References

Alacam, D., & Shilnikov, A. (2015). Making a swim central pattern generator out of latent parabolic bursters. *Int. J. Bifurcation Chaos*, *25*, 540003.

Barnes, C. A., Suster, M. S., Shen, J., & McNaughton, B. L. (1997). Multistability of cognitive maps in the hippocampus of old rats. *Nature*, *388*, 272–275.

Brown, E., Moehlis, J., & Holmes, P. (2004). On the phase reduction and response dynamics of neural oscillator populations. *Neural Computation*, *14*, 673–715.

Buhusi, C. V., & Oprisan, S. A. (2013). Time-scale invariance as an emergent property in a perceptron with realistic, noisy neurons. *Behavioral Processes*, *95*(5), 60–70.

Calvo, O., Chialvo, D. R., Eguiluz, V. M., Mirasso, C., & Toral, R. (2004). Anticipated synchronization: A metaphorical linear view. *Chaos*, *1*, 7–13.

Ciszak, M., Calvo, O., Masoller, C., Mirasso, C. R., & Toral, R. (2003). Anticipating the response of excitable systems driven by random forcing. *Phys. Rev. Lett.*, *90*, 204102.

Destexhe, A., Mainen, Z. F., & Sejnowski, T. J. (1994). Synthesis of models for excitable membranes, synaptic transmission and neuromodulation using a common kinetic formalism. *J. Comput. Neurosci.*, *1*, 195–230.

Eken, T., Hultborn, H., & Kiehn, O. (1989). Possible functions of transmitter-controlled plateau potentials in alpha motoneurons. *Prog. Brain Res.*, *80*, 257–267.

Ermentrout, B. (2002). *Simulating, analyzing, and animating dynamical Systems*. Philadelphia: Society for Industrial and Applied Mathematics.

Ermentrout, G. B. (1996). Type I membranes, phase resetting curves, and synchrony. *Neural Computation*, *8*, 979–1001.

Ermentrout, G. B., Glass, L., & Oldeman, B. E. (2012). The shape of phase-resetting curves in oscillators with a saddle node on an invariant circle bifurcation. *Neural Computation*, *24*, 3111–3125.

FitzHugh, R. (1955). Mathematical models of threshold phenomena in the nerve membrane. *Bull. Math. Biophysics*, *17*, 257–278.

Gray, C. M. (1995). Synchronous oscillations in neuronal systems: Mechanisms and functions. *J. Comput. Neurosci.*, *1*, 11–38.

Izhikevich, E. (2000). Neural excitability, spiking and bursting. *Int. J. Bif. Chaos*, *10*, 1171–1266.

Kirillov, A. B., Myre, C. D., & Woodward, D. J. (1993). Bistability, switches and working memory in a two-neuron inhibitory-feedback model. *Biol. Cybern.*, *68*, 441–449.

Kopell, N., & Somers, D. (1993). Rapid synchronization through fast threshold modulation. *Biol. Cybern.*, *68*, 393–407.

Laurent, G. (1996). Dynamical representation of odors by oscillating and evolving neural assemblies. *Trends Neurosci.*, *19*, 489–496.

Lisman, J. E. (1997). Bursts as a unit of neural information: Making unreliable synapses reliable. *Trends Neurosci.*, *20*, 38–43.

Marder, E., & Calabrese, R. (1996). Principles of rhythmic motor pattern generation. *Physiological Reviews*, *76*, 687–717.

Matias, F. S. (2014). *Anticipated synchronization in neuronal circuits*. PhD thesis, Universidade Federal de Pernambuco, Universitat de les Illes Balears.

Matias, F. S., Carelli, P. V., Mirasso, C. R., & Copelli, M. (2011). Anticipated synchronization in a biologically plausible model of neuronal motifs. *Phys. Rev. E*, *84*, 021922.

Matias, F. S., Carelli, P. V., Mirasso, C. R., & Copelli, M. (2015). Self-organized near-zero-lag synchronization induced by spike-timing dependent plasticity in cortical populations. *PLoS ONE*, *10*, e0140504.

Matias, F. S., Gollo, L. L., Carelli, P. V., Bressler, S. L., Copelli, M., & Mirasso, C. R. (2014). Modeling positive Granger causality and negative phase lag between cortical areas. *NeuroImage*, *99*, 411–418.

McCormick, D. A., & Bal, T. (1997). Sleep and arousal: Thalamocortical mechanisms. *Annu. Rev. Neurosci.*, *20*, 185–215.

Mirollo, R. M., & Strogatz, S. H. (1990). Synchronization of pulse-coupled biological oscillators. *SIAM Journal of Applied Mathematics*, *50*, 1645–1662.

Morris, C., & Lecar, H. (1981). Voltage oscillations in the barnacle giant muscle fiber. *Biophys. J.*, *35*, 193–213.

Nadim, F., Zhao, S., & Bose, A. (2012). A PRC description of how inhibitory feedback promotes oscillation stability. In N. W. Schultheiss, A. A. Prinz, & R. J. Butera (Eds.), *Phase response curves in neuroscience* (vol. 6, pp. 399–417). New York: Springer.

Nagumo, J., Arimoto, S., & Yoshizawa, S. (1962). An active pulse transmission line simulating nerve axon. In *Proceedings of the Institute of Radio Engineers* (vol. 50, pp. 2061–2070).

Netoff, T. I., Acker, C. D., Bettencourt, J. C., & White, J. A. (2005). Beyond two-cell networks: Experimental measurement of neuronal responses to multiple synaptic inputs. *J. Comput. Neurosci.*, *18*, 287–295.

Okamoto, H., & Fukai, T. (2000). A model for neural representation of temporal duration. *Biosystems*, *55*, 59–64.

Oprisan, S. A. (2009). Stability of synchronous oscillations in a periodic network. *International Journal of Neuroscience*, *4*, 482–491.

Oprisan, S. A. (2010). Existence and stability criteria for phase-locked modes in ring neural networks based on the spike time resetting curve method. *Journal of Theoretical Biology*, *262*, 232–244.

Oprisan, S. A. (2012a). Existence and stability criteria for phase-locked modes in ring networks using phase-resetting curves and spike time resetting curves. In N. W. Schultheiss, A. A. Prinz, & R. J. Butera (Eds.), *Phase response curves in neuroscience* (vol. 6, pp. 419–451). New York: Springer.

Oprisan, S. A. (2012b). A geometric approach to phase resetting estimation based on mapping temporal to geometric phase. In N. W. Schultheiss, A. A. Prinz, & R. J. Butera (Eds.), *Phase response curves in neuroscience* (vol. 6, pp. 131–162). New York: Springer.

Oprisan, S. A. (2013). All phase resetting curves are bimodal, but some are more bimodal than others. *ISRN Computational Biology*, *2013*, 230571.

Oprisan, S. A. (2014a). Local linear approximation of the Jacobian matrix better captures phase resetting of neural limit cycle oscillators. *Neural Computation*, *26*, 1132–157.

Oprisan, S. A. (2014b). Multistability of coupled neuronal oscillators. In J. Dieter & J. Ranu (Eds.), *Encyclopedia of computational neuroscience* (pp. 1–15). New York: Springer.

Oprisan, S. A., & Boutan, C. (2008). Prediction of entrainment and 1:1 phase-locked modes in two-neuron networks based on the phase resetting curve method. *International Journal of Neuroscience*, *6*, 867–890.

Oprisan, S. A., & Buhusi, C. V. (2011). Modeling pharmacological clock and memory patterns of interval timing in a striatal beat-frequency model with realistic, noisy neurons. *Frontiers in Integrative Neuroscience*, *52*, 1–11.

Oprisan, S. A., & Buhusi, C. V. (2013a). How noise contributes to time-scale invariance of interval timing. *Phys. Rev. E*, *87*(5), 052717.

Oprisan, S. A., & Buhusi, C. V. (2013b). Why noise is useful in functional and neural mechanisms of interval timing? *BMC Neuroscience*, *14*(1), 1–12.

Oprisan, S. A., & Buhusi, C. V. (2014). What is all the noise about in interval timing? *Philosophical Transactions of the Royal Society B: Biological Sciences*, *369*, 20120459.

Oprisan, S. A., & Canavier, C. C. (2002a). The influence of limit cycle topology on the phase resetting curve. *Neural Computation*, *14*(5), 1027–1057.

Oprisan, S. A., & Canavier, C. C. (2002b). Stability analysis of rings of pulse-coupled oscillators: The effect of phase resetting in the second cycle after the pulse is important at synchrony and for long pulses. *Journal of Differential Equations and Dynamical Systems*, *3–4*, 243–258.

Oprisan, S. A., & Canavier, C. C. (2003). Stability analysis of entrainment by two periodic inputs with a fixed delay. *Neurocomputing*, *52–54*, 59–63.

Oprisan, S. A., & Canavier, C. C. (2005). Stability criterion for a two-neuron reciprocally coupled network based on the phase and burst resetting curves. *Neurocomputing*, *65–66*, 733–739.

Oprisan, S. A., Dix, S., & Buhusi, C. V. (2014). Phase resetting and its implications for interval timing with intruders. *Behavioral Processes*, *101*, 146–153.

Oprisan, S. A., Lynn, P. E., Tompa, T., & Lavin, A. (2015). Low-dimensional attractor for neural activity from local field potentials in optogenetic mice. *Front. Comput. Neurosci.*, *8*, 125.

Oprisan, S. A., Prinz, A. A., & Canavier, C. C. (2004). Phase resetting and phase locking in hybrid circuits of one model and one biological neuron. *Biophysical Journal*, *87*, 2283–2298.

Oprisan, S. A., Thirumalai, V., & Canavier, C. C. (2003). Dynamics from a time series: Can we extract the phase resetting curve from a time series? *Biophysical Journal*, *84*, 2919–2928.

Perkel, D. H., Schulman, J. H., Bullock, T. H., Moore, G. P., & Segundo, J. P. (1964). Pacemaker neurons: Effects of regularly spaced synaptic input. *Science*, *145*, 61–63.

Pervouchine, D. D., Netoff, T. I., Rotstein, H. G., White, J. A., Cunningham, M. O., Whittington, M. A., & Kopell, N. J. (2006). Low dimensional maps encoding dynamics in entorhinal cortex and hippocampus. *Neural Comput.*, *18*, 2617–2650.

Plant, R. E., & Kim, M. (1976). Mathematical description of a bursting pacemaker neuron by a modification of the Hodgkin-Huxley equations. *Biophys. J.*, *16*, 227–244.

Refinetti, R. (2005). *Circadian physiology*. Boca Raton, FL: CRC Press.

Romei, V., Gross, J., & Thut, G. (2012). Sounds reset rhythms of visual cortex and corresponding human visual perception. *Current Biology*, *22*(9), 807–813.

Sakurai, A., Gunaratne, C. A., & Katz, P. S. (2014). Two interconnected kernels of reciprocally inhibitory interneurons underlie alternating left-right swim motor pattern generation in the mollusk *Melibe leonina*. *Journal of Neurophysiology*, *112*, 1317–1328.

Sausedo-Solorio, J. M., & Pisarchik, A. N. (2014). Synchronization of map-based neurons with memory and synaptic delay. *Physics Letters A*, *378*(30–31), 2108–2112.

Schwabedal, J. T. C., Knapper, D. E., & Shilnikov, A. L. (2016). Qualitative and quantitative stability analysis of penta-rhythmic circuits. *Nonlinearity*, *29*(12), 3647–3663.

Selverston, A. (1987). *Model neural networks and behavior*. Berlin: Springer.

Shilnikov, A., Gordon, R., & Belykh, I. (2008). Polyrhythmic synchronization in bursting networking motifs. *Chaos*, *18*, 037120-1–037120-13.

Simonov, A. Y., Gordleeva, S. Y., Pisarchik, A. N., & Kazantsev, V. B. (2014). Synchronization with an arbitrary phase shift in a pair of synaptically coupled neural oscillators. *JETP Letters*, *98*(10), 632–637.

Skinner, F. K., Bazzazi, H., & Campbell, S. A. (2005). Two-cell to n-cell heterogeneous, inhibitory networks: Precise linking of multi-stable and coherent properties. *J. Comput. Neurosci.*, *18*, 343–352.

Stephan, K. E., Zilles, K., & Kotter, R. (2000). Coordinate-independent mapping of structural and functional data by objective relational transformation (ORT). *Philos. Trans. R. Soc. Lond. B Biol. Sci.*, *355*, 37–54.

Stepp, N., & Turvey, M. T. (2010). On strong anticipation. *Cognitive Systems Research*, *11*(2), 148–164.

Vetter, G., Haynes, J. D., & Pfaff, S. (2000). Evidence for multistability in the visual perception of pigeons. *Vision Res.*, *40*, 2177–2186.

Vollmer, M. K., Vanderweyen, C. D., Tuck, D. R., & Oprison, S. A. (2015). Predicting phase resetting due to multiple stimuli. *Journal of the South Carolina Academy of Science*, *13*(5), 1–7.

Voss, H. U. (2000). Anticipating chaotic synchronization. *Phys. Rev. E*, *61*(5), 5115–5119.

Winfree, A. (2001). *The geometry of biological time*. New York: Springer-Verlag.

Winfree, A. T. (1989). Electrical instability in cardiac muscle: Phase singularities and rotors. *Journal of Theoretical Biology*, *138*, 353–405.

Received December 24, 2016; accepted March 8, 2017.